

AIR FORCE REPORT NO.  
SAMSO-TR-74-118

*Theoretical Notes*  
*Note 267*

AEROSPACE REPORT NO.  
TR-0074 (4124) -3

*TN 267*

## Space Charge Limiting from Blackbody Radiation

*Gerald G. Comisar*

Prepared by G. G. COMISAR  
Materials Sciences Laboratory

14 May 1974

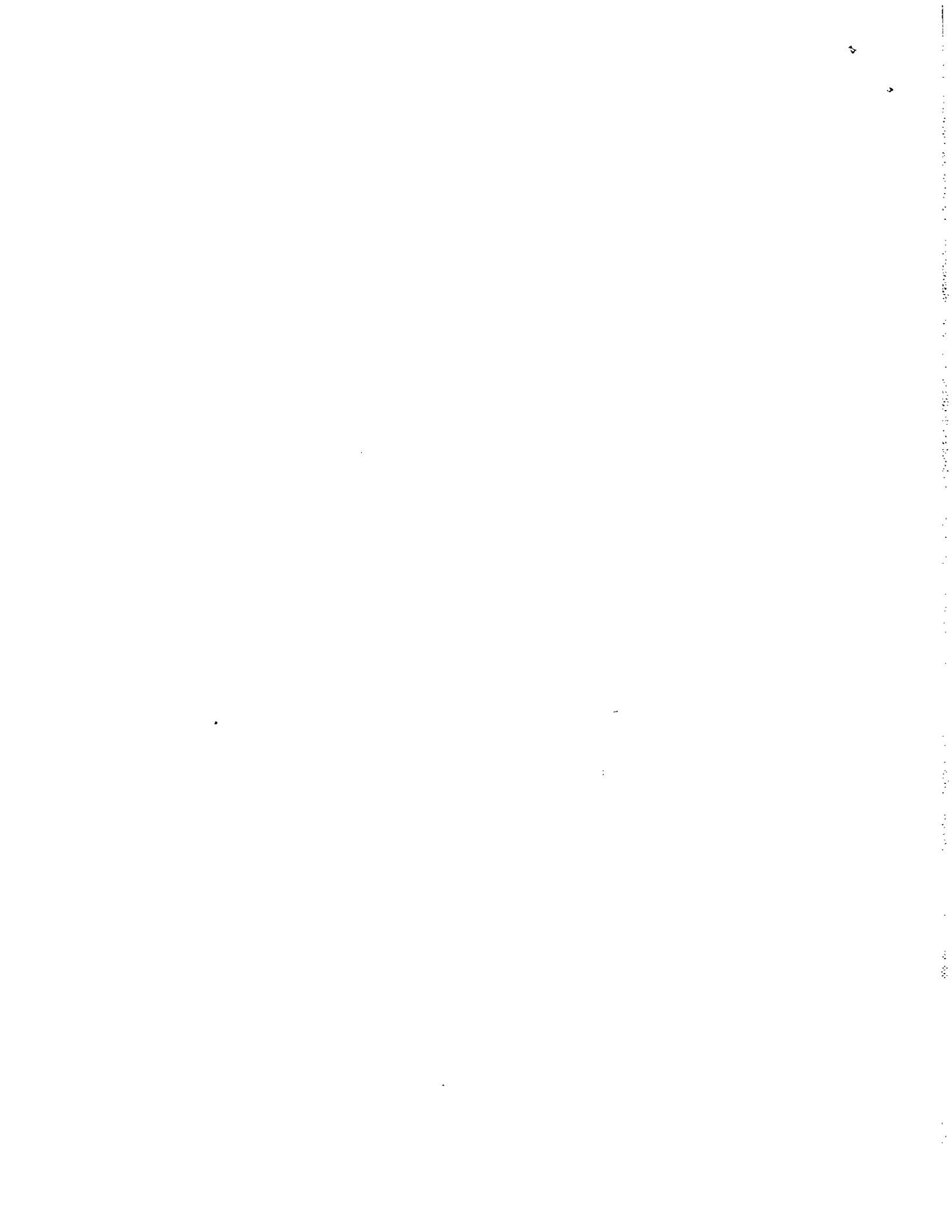
---

Technology Division  
THE AEROSPACE CORPORATION

---

Prepared for SPACE AND MISSILE SYSTEMS ORGANIZATION  
AIR FORCE SYSTEMS COMMAND  
LOS ANGELES AIR FORCE STATION  
Los Angeles, California

APPROVED FOR PUBLIC RELEASE: DISTRIBUTION UNLIMITED



## FOREWORD

This report is published by The Aerospace Corporation, El Segundo, California under Air Force Contract No. F04701-73-C-0074.

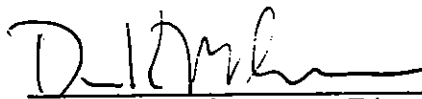
The report, which documents research carried out from March 1973 through May 1973, was submitted on 17 April 1974 to Major Larry A. Darda, DYAE, for review and approval.

Approved



---

W. C. Riley, Director  
Materials Sciences Laboratory  
Laboratory Operations



---

D. A. McPherson, Director  
Survivability Directorate  
Technology Division  
Development Operations

Publication of this report does not constitute Air Force approval of the report's findings or conclusions. It is published only for the exchange and stimulation of ideas.



---

Larry A. Darda, Major, USAF  
Project Officer  
Survivability Directorate

## ABSTRACT

A grounded, parallel-plate vacuum diode illuminated by x rays generates a two-sided distribution of non-Maxwellian photoelectrons. The resulting potential hill problem may be reduced to a first-order nonlinear differential equation subject to two-point boundary conditions. An iterative APL/360 program has been written to allow the user to perform on-line calculations of potentials. Numerical results are presented for several cases of incident blackbody radiation and unequal two-sided emission.

## CONTENTS

FOREWORD . . . . .	iii
ABSTRACT . . . . .	iv
I. INTRODUCTION . . . . .	1
II. BASIC EQUATIONS . . . . .	3
III. METHODS OF SOLUTION . . . . .	11
IV. MODEL ELECTRON ENERGY DISTRIBUTIONS FOR BLACKBODY RADIATION . . . . .	13
V. NUMERICAL RESULTS . . . . .	21
REFERENCES . . . . .	37

## FIGURES

1.	Geometry of a Parallel Plate Diode of Plate Thickness $d$ and Spacing $\ell$ Emitting Current Densities $J_1$ and $J_2$ A/cm <sup>2</sup> under Irradiation by Filtered Blackbody Photons . . . . .	4
2(a).	Blackbody Current Distribution Fit to a Triangular Model ( $T_{BB} = 5$ keV, $d = 2$ mm Al) . . . . .	16
2(b).	Blackbody Current Distribution Fit to a Triangular Model ( $T_{BB} = 10$ keV, $d = 2$ mm Al) . . . . .	17
2(c).	Blackbody Current Distribution Fit to a Triangular Model ( $T_{BB} = 20$ keV, $d = 2$ mm Al) . . . . .	18
3.	Listing of APL Programs . . . . .	23
4.	Printout of Typical Terminal Session . . . . .	29
5.	Potential Curves for Symmetric Diode with $J_0 \ell^2$ as a Parameter . . . . .	31
6.	Potential Curves with $\kappa$ as a Parameter . . . . .	32

## TABLES

1.	Summary of Model Parameters for Triangular Current Distributions . . . . .	19
2.	Peak Potentials and Net Currents for a Single Diode . . . . .	33
3.	Peak Potentials from a Symmetric Double Diode . . . . .	34

## I. INTRODUCTION

The study of space charge limiting in single and double diodes arose early in electron physics in connection with thermionic emission. The substantial body of work generated by Langmuir and others is surveyed in the review article by Ivey (Ref. 1). Time-dependent effects such as instabilities have been developed in detail by Birdsall and Bridges (Ref. 2).

Currently, there is considerable interest in the response of electronic systems to intense photon environments for which  $h\nu = 1$  to 100 keV. Of particular interest are internal electromagnetic pulse (IEMP) phenomena generated by photoelectron emission in metallic cavities. The earlier works cited deal almost exclusively with Maxwellian photoelectron energy distributions. However, recent measurements (Ref. 3) and Monte Carlo calculations (Ref. 4) reveal that photoelectron distributions for monochromatic photons are actually triangular rather than Gaussian. Furthermore, in realistic IEMP cavities, emission from opposing walls is important, and the two-ended emitter (double diode) problem must be solved. For Maxwellian distributions, the double-diode problem reduces to a fairly simple statistical mechanics calculation, but, for the triangular electron distributions, this approach is no longer valid. An additional complication is that realistic radiation spectra tend to be filtered Planckian rather than monochromatic and, hence, the triangular photoelectron distributions must be summed over a broad photon spectrum.

Recently, Wenaas and co-workers (Ref. 5) developed one-dimensional and two-dimensional computer codes for the one-sided (single diode) problem. In the present report, the planar double-diode problem is investigated for filtered blackbody photon spectra. Stationary potential equations are developed under the assumption of zero ambient air pressure and nonrelativistic electron trajectories. A model photoelectron current distribution is introduced and used to simplify the equations governing electric field and

net current. The resulting differential equation is solved numerically by a Runge-Kutta procedure programmed for on-line use with IBM remote terminals. Execution time per double-diode case turns out to compare favorably with previous single-diode work.



## II. BASIC EQUATIONS

Consider a pair of grounded parallel plates located at  $x = 0$  and  $x = \ell$ , respectively. The space between the plates is assumed to be a vacuum. Let us assume that, under the action of x-ray bombardment or some other electron generation mechanism, the two plates emit electric currents with electron energy distributions  $J_1(E) dE$  and  $J_2(E) dE$  (see Fig. 1). Each electron energy group contributes a space charge density given by  $\rho(E) = J(E)/v_e$  where the electron velocity  $v_e$  is related to the electric potential  $V(x)$  by the nonrelativistic energy conservation relation

$$\frac{1}{2} m v_e^2 + eV(x) = E \quad (1)$$

The electric potential is obtained by solving the Poisson equation

$$\frac{d^2 V(x)}{dx^2} = - \frac{1}{\epsilon_0} \rho(x) \quad (2)$$

subject to the grounded plate conditions  $V(0) = V(\ell) = 0$ .

The net effect of the motion of electrons in the space charge field is to form a potential hill of height  $V = V_M$  located at  $x = x_M$ . Lower energy electrons are repelled back into the emitting plates while the higher energy electrons escape over the top of the potential barrier and are collected on the opposite plate. For simplicity we neglect any electron reflection and re-emission after collection.

On the left side of the hill ( $x < x_M$ ), the net current  $J_n$  consists of a forward component  $J_{f1}$ , a backward component  $J_{b1}$ , and an additional component  $J_{f2}$  arising from electrons arriving from the right side, namely:

$$J_n = J_{f1} - J_{b1} - J_{f2} \quad (3)$$

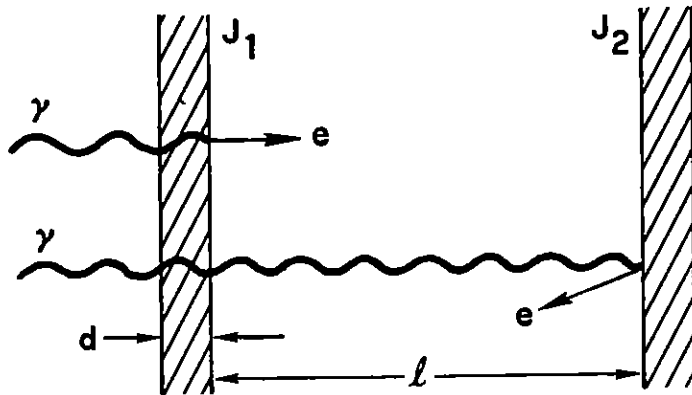


Fig. 1. Geometry of a Parallel Plate Diode of Plate Thickness  $d$  and Spacing  $l$  Emitting Current Densities  $J_1$  and  $J_2$  A/cm<sup>2</sup> under Irradiation by Filtered Blackbody Photons

where  $J_n$  is constant because of the continuity equation  $dJ/dx = 0$ . Each individual current contribution varies spatially with  $V(x)$  according to

$$J_{f1}(x) = \int_{eV(x)}^{\infty} J_1(E) dE \quad (4a)$$

$$J_{b1}(x) = \int_{eV(x)}^{eV_M} J_1(E) dE \quad (4b)$$

and

$$J_{f2}(x) = \int_{eV_M}^{\infty} J_2(E) dE \quad (4c)$$

As expected, the net current is just

$$J_n = \int_{eV_M}^{\infty} [J_1(E) - J_2(E)] dE \quad (5)$$

Similar arguments apply on the right side of the potential hill ( $x > x_M$ ) after exchanging the subscripts 1 and 2. From the conservation of current and energy, we obtain the following space charge density

$$\begin{aligned} \rho(x) &= \rho_{f1} + \rho_{b1} + \rho_{f2} \\ &= \int_{eV(x)}^{\infty} \frac{dE J_1(E)}{\left[\frac{2}{m}(E - eV(x))\right]^{1/2}} + \int_{eV(x)}^{eV_M} \frac{dE J_1(E)}{\left[\frac{2}{m}(E - eV(x))\right]^{1/2}} \\ &\quad + \int_{eV_M}^{\infty} \frac{dE J_2(E)}{\left[\frac{2}{m}(E - eV(x))\right]^{1/2}} \end{aligned} \quad \begin{array}{l} (6a) \\ (Cont.) \end{array}$$

$$= 2 \int_{eV(x)}^{\infty} \frac{dE J_1(E)}{\left[\frac{2}{m}(E - eV(x))\right]^{1/2}} - \int_{eV_M}^{\infty} \frac{dE[J_1(E) - J_2(E)]}{\left[\frac{2}{m}(E - eV(x))\right]^{1/2}} \text{ for } x \leq x_M \quad (6a)$$

and

$$\rho(x) = 2 \int_{eV(x)}^{\infty} \frac{dE J_2(E)}{\left[\frac{2}{m}(E - eV(x))\right]^{1/2}} + \int_{eV_M}^{\infty} \frac{dE[J_1(E) - J_2(E)]}{\left[\frac{2}{m}(E - eV(x))\right]^{1/2}} \text{ for } x \geq x_M \quad (6b)$$

Note that the space charge density  $\rho$  is continuous across the potential hill; i. e.,  $\rho = \rho_{f1} + \rho_{f2}$  at  $V = V_M$ .

To reduce the second-order system consisting of Eqs. (2) and (6) to a first-order system, multiply both sides of (2) by  $dV/dx$  and integrate to obtain

$$\frac{1}{2} \left( \frac{dV}{dx} \right)^2 = \frac{1}{\epsilon_0} \int_{V_M}^{V(x)} dV' \int_0^{\infty} \rho(E, V') dE \quad (7)$$

where the integration constant has been chosen so that  $dV/dx = 0$  at  $V = V_M$ . After some algebra, it can be shown that

$$\left( \frac{dV}{dx} \right)^2 = \frac{1}{\epsilon_0 e} \frac{4}{(2/m)^{1/2}} \left\{ 2 \int_{eV}^{\infty} dE J_1(E) (E - eV)^{1/2} - 2 \int_{eV_M}^{\infty} dE J_1(E) (E - eV_M)^{1/2} \right. \\ \left. - \int_{eV_M}^{\infty} dE [J_1(E) - J_2(E)] [(E - eV)^{1/2} - (E - eV_M)^{1/2}] \right\} \\ \text{for } x \leq x_M \quad (8a)$$

and

$$\left(\frac{dV}{dx}\right)^2 = \frac{1}{\epsilon_0 e} \frac{4}{(2/m)^{1/2}} \left\{ 2 \int_{eV}^{\infty} dE J_2(E) (E - eV)^{1/2} - 2 \int_{eV_M}^{\infty} dE J_2(E) (E - eV_M)^{1/2} \right. \\ \left. - \int_{eV_M}^{\infty} dE [J_2(E) - J_1(E)] [(E - eV)^{1/2} - (E - eV_M)^{1/2}] \right\} \\ \text{for } x \geq x_M \quad (8b)$$

These solutions may be verified by direct differentiation and comparison with the original differential Eqs. (2) and (6).

Introducing the dimensionless variables

$$x = l\xi \qquad V = V_0 \nu \\ J_1(E) dE = J_0 j_1(\eta) d\eta \qquad J_2(E) dE = J_0 j_2(\eta) d\eta \quad (9)$$

where  $J_0$  is chosen such that  $\int_0^{\infty} j_1(\eta) d\eta = 1$ , we obtain the dimensionless differential equations

$$\left(\frac{d\nu}{d\xi}\right)^2 = \frac{16}{9} \left\{ 2 \int_{\nu}^{\infty} d\eta j_1(\eta) (\eta - \nu)^{1/2} - 2 \int_{\nu_M}^{\infty} d\eta j_1(\eta) (\eta - \nu_M)^{1/2} \right. \\ \left. - \int_{\nu_M}^{\infty} d\eta [j_1(\eta) - j_2(\eta)] [(\eta - \nu)^{1/2} - (\eta - \nu_M)^{1/2}] \right\} \text{for } x < x_M \quad (10a)$$

and

$$\left(\frac{dv}{d\xi}\right)^2 = \frac{16}{9} \left\{ 2 \int_{\nu}^{\infty} d\eta j_2(\eta) (\eta - \nu)^{1/2} - 2 \int_{\nu_M}^{\infty} d\eta j_2(\eta) (\eta - \nu_M)^{1/2} \right. \\ \left. + \int_{\nu_M}^{\infty} d\eta [j_1(\eta) - j_2(\eta)] [(\eta - \nu)^{1/2} - (\eta - \nu_M)^{1/2}] \right\} \text{ for } x > x_M \quad (10b)$$

in which the potential scaling factor is obtained from the Child-Langmuir law

$$V_o = \left[ \frac{9}{4} \ell^2 \frac{J_o}{\epsilon_o} \frac{1}{(2 e/m)^{1/2}} \right]^{2/3} = 5.69 (J_o \ell^2)^{2/3} \text{ kV} \quad (10c)$$

The two-point boundary conditions are now  $\nu = 0$  at  $\xi = 0$  and 1.

For the case of a symmetric double diode ( $j_1 = j_2$ ), the two differential equations become identical, as expected. The only explicit parameter in Eq. (10) is the barrier height  $\nu_M = V_M/V_o$ , in which  $V_o$  in turn depends on the scaling parameter  $J_o \ell^2$ . The current distributions  $j_1$  and  $j_2$  depend implicitly on  $J_o \ell^2$  and other additional physical quantities such as radiation temperature and emitter composition.

In the special case where the forward and backward emission spectra of the photoelectrons are equal, we may write  $j_1 = j$  where  $\int_0^{\infty} j(\eta) d\eta = 1$  and  $j_2 = \kappa j$ , the function  $\kappa$  now reducing to a constant independent of electron energy. This allows the basic equations to be written in the more concise form:

$$\left(\frac{dv}{d\xi}\right)^2 = \frac{16}{9} \left\{ 2 F_1 + (1 + \kappa) F_2 \right\} \quad \text{for } x \leq x_M \quad (11a)$$

$$\left(\frac{dv}{d\xi}\right)^2 = \frac{16}{9} \left\{ 2 \kappa F_1 + (1 + \kappa) F_2 \right\} \quad \text{for } x \geq x_M \quad (11b)$$

where

$$F_1 = \int_{\nu}^{\nu_M} d\eta j(\eta) (\eta - \nu)^{1/2}$$
$$F_2 = \int_{\nu_M}^{\infty} d\eta j(\eta) [(\eta - \nu)^{1/2} - (\eta - \nu_M)^{1/2}] \quad (11c)$$

)

.

.

.

)

.

.

)



### III. METHODS OF SOLUTION

The second-order Poisson equation has been reduced to the form  $d\nu/d\xi = F(\nu)$ . Integration yields the formal solution

$$\xi = \int_0^\nu \frac{d\nu}{F(\nu)} \quad (12)$$

which satisfies the equation  $\nu = 0$  at  $\xi = 0$ . Furthermore, the peak potential  $\nu_M$  must be chosen to satisfy the other condition  $\nu = 0$  at  $\xi = 1$ . For certain current distributions, the resulting charge density function  $F(\nu)$  is sufficiently simple for the integral (12) to be explicitly performed. However, this usually does not facilitate matters since a solution of the form  $\xi = G(\nu)$  must still be inverted to give the desired potential curve  $\nu = G^{-1}(\xi)$ . This inversion must generally be done numerically or graphically.

If we adopt the strategy of directly integrating Eq. (12) numerically, another difficulty arises because of the singularity at  $F(\nu_M) = 0$ . Expansion of the right-hand sides of Eqs. (11) about  $\nu = \nu_M$  for actual current distributions reveals the integral contribution

$$\int_{(1-\epsilon)\nu_M}^{\nu_M} \frac{d\nu}{F(\nu)}$$

to be of the order  $\epsilon^{1/2}$ . Consequently, small values of  $\epsilon$  must be chosen, implying a correspondingly small step size in the numerical integration. Such computer runs are excessively time consuming, and thus the differential equation approach appears preferable.

The numerical results given here were obtained by means of the APL/360 routine RUNGE provided by Dr. D. C. Pridmore-Brown. This

is a Runge-Kutta procedure whose step size and format are controlled by the vector  $V$  (not to be confused with potential) and which operates on the differential equation defined by the function SET. (The detailed documentation is available from the writer on request.) It is most convenient to integrate Eqs. (10a) and (10b) simultaneously from  $\nu \approx \nu_M$  out to  $\nu \approx 0$  rather than integrate the individual halves of the potential consecutively. This results in a substantial saving in computing time. Further time can be saved by choosing the fairly large step size  $\Delta\xi = 0.05$ . We estimate that this subdivision introduces errors of around 2 percent in the potential solutions and around 6 percent in the values for net current.

The method has been checked for the one-sided case by passing to the limit of vanishingly small barrier heights ( $\nu_M \rightarrow 0$ ). As  $\nu_M$  diminishes, the potential curves become parabolic with distance  $\xi$ , in agreement with the linear small-field approximation  $d^2V/dx^2 = -J/\epsilon_0 v_e$ . In the opposite limit of increasing barrier heights, the potential curve becomes increasingly skewed toward the left, approaching a thin sheath with a linear tail in agreement with the vacuum approximation  $d^2V/dx^2 = 0$ .

Solutions have been studied by the writer for x-ray spectra that are monoenergetic, flat, or ideal blackbody (Planckian). Only the case of blackbody radiation will be presented in this report. The basic equations (10) can also be readily used to handle input data on photoelectron spectra originating from measurements or from Monte Carlo computer runs. The integrals over electron energy would then be replaced by finite summations with judiciously selected quadrature weighing coefficients.

#### IV. MODEL ELECTRON ENERGY DISTRIBUTIONS FOR BLACKBODY RADIATION

The photoelectron current produced by incident x rays is the product of the filtered photon flux at the emitter surface times the photoelectric production cross section summed over all photon energies. The ideal blackbody spectrum is given by the Planck formula

$$N(E_\gamma) dE_\gamma = \frac{CE_\gamma^2 dE_\gamma}{\exp(E_\gamma/T) - 1} \quad (13)$$

where  $E_\gamma = h\nu$  is the photon energy in keV,  $T$  is the blackbody temperature in keV, and  $C$  is a normalization constant chosen such that  $\int_0^\infty N(E) dE = 1$ . An attenuation factor  $\exp[-\rho d \mu(E_\gamma)]$  must be inserted for an emitter of mass  $\rho d$  ( $\text{g/cm}^2$ ) and total mass absorption coefficient  $\mu \text{ cm}^2/\text{g}$ . The photoelectron production cross section is proportional to the amount of photoelectric absorption of incident photons:  $[1 - \exp(-R_e \mu)] \approx R_e \mu$ , where  $R_e$  is the electron stopping range in  $\text{g/cm}^2$ . Strictly speaking, we should also include an energy-dependent factor to account for multiple scattering of electrons within the emitter. However, for sufficiently low atomic number and photon energy, this variation in energy is relatively slow (Ref. 6). Above the K-edge for the emitter, the photoelectric absorption to a good approximation varies as  $(E_\gamma - E_K)^{-3}$ , while the electron range varies as  $(E_\gamma - E_K)^2$  (see Ref. 7). A final ingredient is the electron energy spectrum for monochromatic photons. The measurements of Denisov (Ref. 3) reveal the dominant contribution to the photoelectron energy spectra of light elements ( $E_K \ll h\nu$ ) to be linear up to the maximum photoelectron energy  $E_\gamma - E_K$ . Combining all of these ingredients, we get, for the blackbody photoelectron current spectrum,

$$\begin{aligned}
J(E) dE &= C' \int_{E+E_K}^{\infty} \frac{E_Y^2 \exp[-\rho d \mu(E_Y)]}{\exp(E_Y/T) - 1} \cdot \frac{dE_Y}{(E_Y - E_K)^3} \\
&\quad \cdot (E_Y - E_K)^2 \cdot \frac{E dE}{(E_Y - E_K)^2} \\
&= C' E dE \int_{E+E_K}^{\infty} dE_Y \frac{\exp[-(E_\ell/E_Y)^3]}{\exp(E_Y/T) - 1} \frac{E_Y^2}{(E_Y - E_K)^3} \quad (14)
\end{aligned}$$

where  $E_Y = E_\ell$  is equivalent to the e-fold attenuation factor corresponding to  $\rho d \mu = 1$ . The factor  $C'/(E_Y - E_K)^2$  is introduced to normalize the total electron spectrum to unity. If we continue to neglect K-edge effects ( $E_K \ll h\nu$ ), and introduce the dimensionless variables

$$\begin{aligned}
\eta &= E/V_0 & \eta_\ell &= E_\ell/V_0 \\
\beta &= V_0/T & x &= E_Y/E \\
y &= \eta\beta = E/T & y_\ell &= E_\ell/T \dots \quad (15a)
\end{aligned}$$

we obtain the dimensionless form for Eq. (14),

$$j(\eta) = C J(\eta\beta) \quad (15b)$$

where

$$J(y) = y \int_1^{\infty} \frac{dx}{x} \frac{\exp[-(y_\ell/xy)^3]}{\exp xy - 1} \dots \quad (15c)$$

The function  $J(y)$  exhibits fairly simple behavior:

$$\begin{aligned} J(y) &\sim y && \text{for } y \rightarrow 0 \\ &\sim \exp(-y) && \text{for } y \rightarrow \infty \end{aligned} \quad (16)$$

which can be verified by asymptotic expansions of Eq. (15c). Some typical computer plots are shown in Fig. 2 for the case of  $0.54 \text{ g/cm}^2$  of aluminum and  $T = 5, 10, \text{ and } 20 \text{ keV}$ . A useful approximation is the triangular distribution sketched on each plot, for which the governing parameters are  $y_1$  and  $y_2$ . This model distribution function is used in the remainder of this discussion. A summary of model parameters is presented in Table 1.

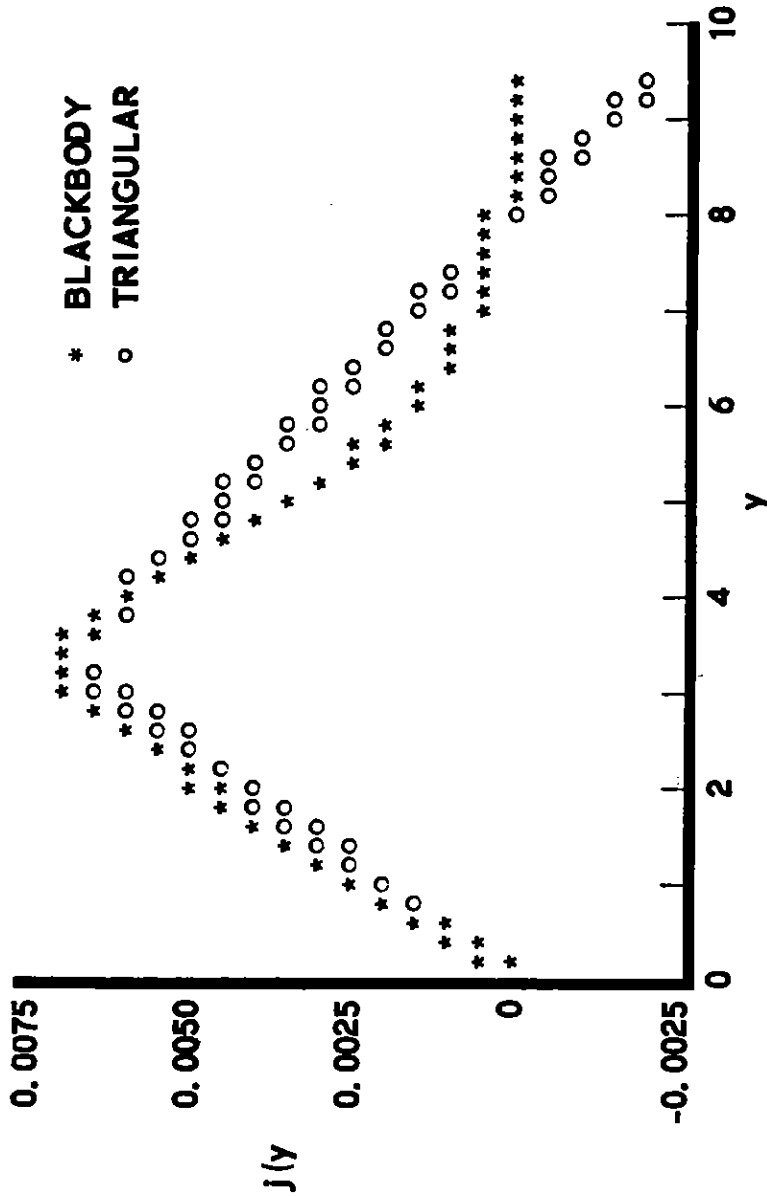
In analytic form, the triangular distribution may be written as

$$\begin{aligned} j(\eta) &= \frac{2}{\eta_2} \frac{\eta}{\eta_1} && \text{for } \eta \leq \eta_1 = \frac{y_1}{\beta} \\ &= \frac{2}{\eta_2} \frac{\eta_2 - \eta}{\eta_2 - \eta_1} && \text{for } \eta_1 \leq \eta \leq \eta_2 = \frac{y_2}{\beta} \end{aligned} \quad (17)$$

It is not difficult to establish directly that  $\int_0^\infty j(\eta) d\eta = 1$ , as required in Section II. The net current is

$$\begin{aligned} J_n / J_o &= (1 - \kappa) \int_{\nu_M}^{\infty} j(\eta) d\eta \\ &= (1 - \kappa) \left[ 1 - \left( \frac{\nu_M}{\eta_1} \right)^2 \frac{\eta_1}{\eta_2} \right] && \text{for } 0 \leq \nu_M \leq \eta_1 \\ &= (1 - \kappa) \frac{\left( 1 - \frac{\nu_M}{\eta_1} \frac{\eta_1}{\eta_2} \right)^2}{1 - \eta_1 / \eta_2} && \text{for } \eta_1 \leq \nu_M \leq \eta_2 \end{aligned} \quad (18)$$

TBB+5  
 MODELFIT  
 SPECIFY MASS OF EMITTER IN G/CM\*2.  
 □: MASS  
 IS A PLOT REQUIRED(YES OR NO)?  
 YES

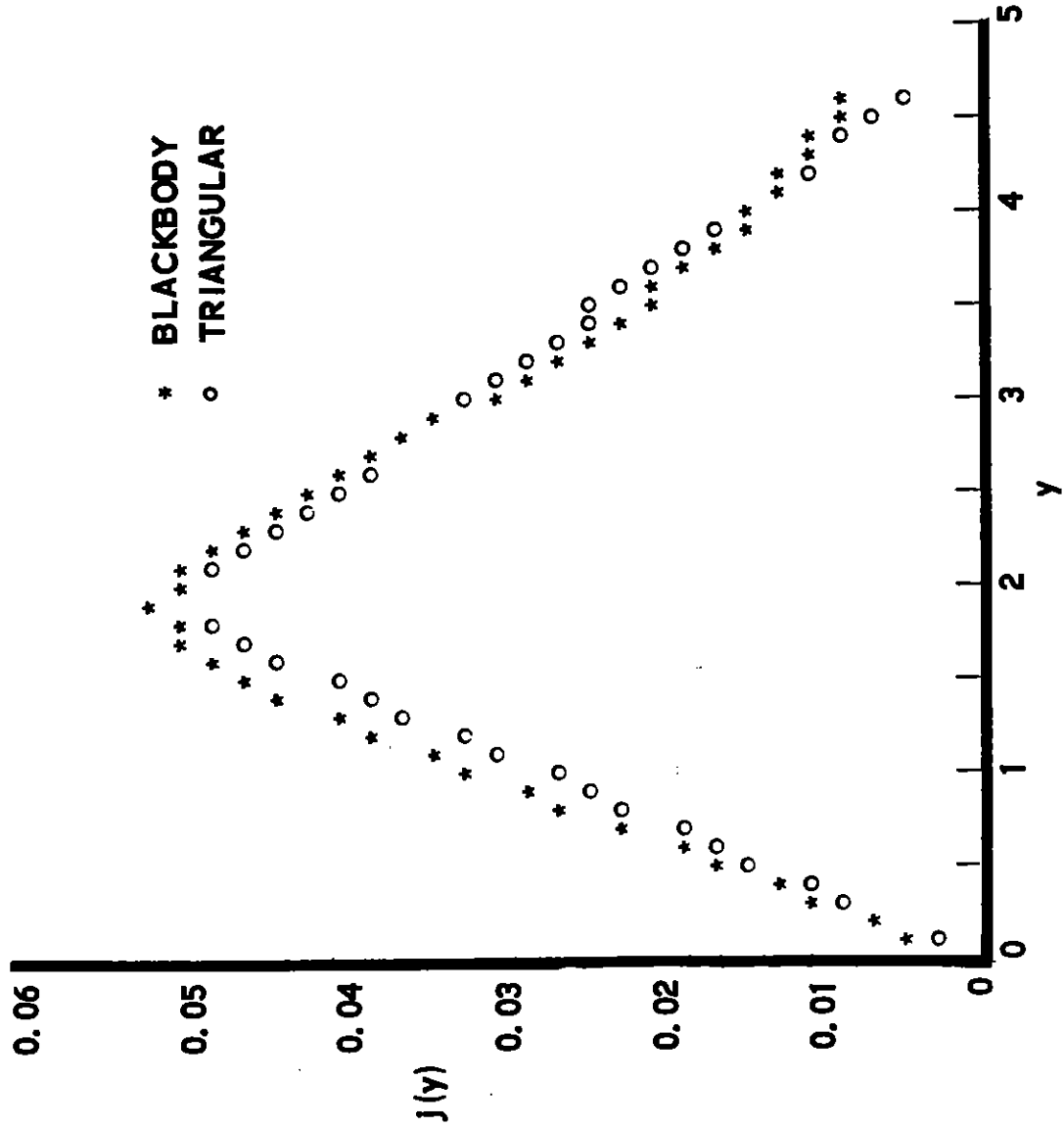


TBB= 5    Y1= 3.3    Y2= 8.0025    YL= 4.661    MASS= 0.538    (G/CM\*2)

Fig. 2(a). Blackbody Current Distribution Fit to a Triangular Model  
 ( $T_{BB} = 5 \text{ keV}$ ,  $d = 2 \text{ mm Al}$ )

MODELPIT  
 SPECIFY MASS OF EMITTER IN G/CM\*2.

Q: MASS  
 IS A PLOT REQUIRED (YES OR NO)?  
 YES



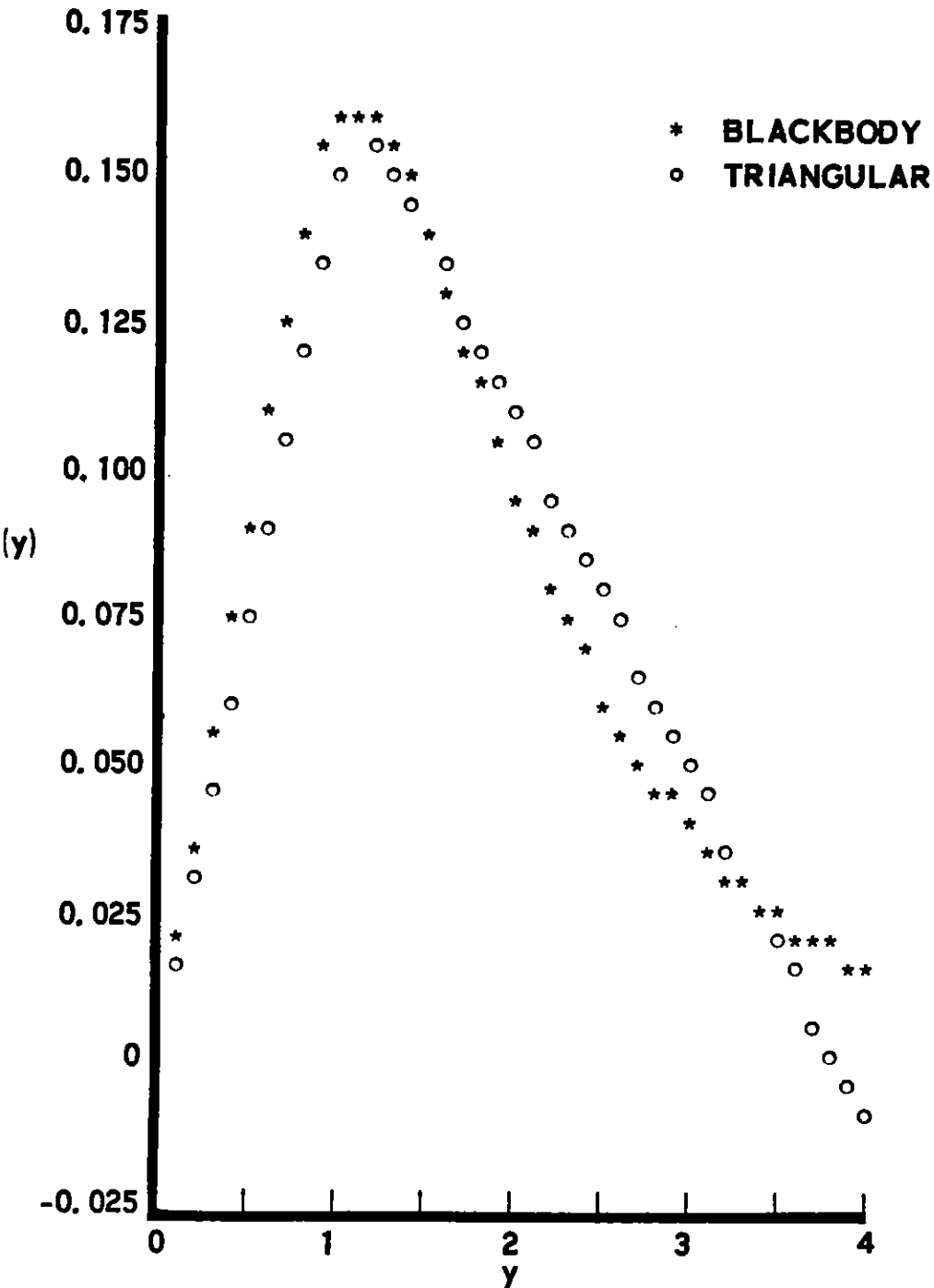
TBB= 10    Y1= 1.9    Y2= 4.8182    YL= 2.3305    MASS= 0.538    (G/CM\*2)

Fig. 2(b). Blackbody Current Distribution Fit to a Triangular Model  
 ( $T_{BB} = 10$  keV,  $d = 2$  mm Al)

PLOTPARM+35  
MODELFIT

SPECIFY MASS OF EMITTER IN G/CM\*2.

□:  
MASS  
IS A PLOT REQUIRED(YES OR NO)?  
Y



TBB= 20 Y1= 1.1 Y2= 3.8109 YL= 1.1653 MASS(G/CM\*2)= 0.538  
PLOT SCALE= 35

Fig. 2(c). Blackbody Current Distribution Fit to a Triangular Model  
( $T_{BB} = 20$  keV,  $d = 2$  mm Al)

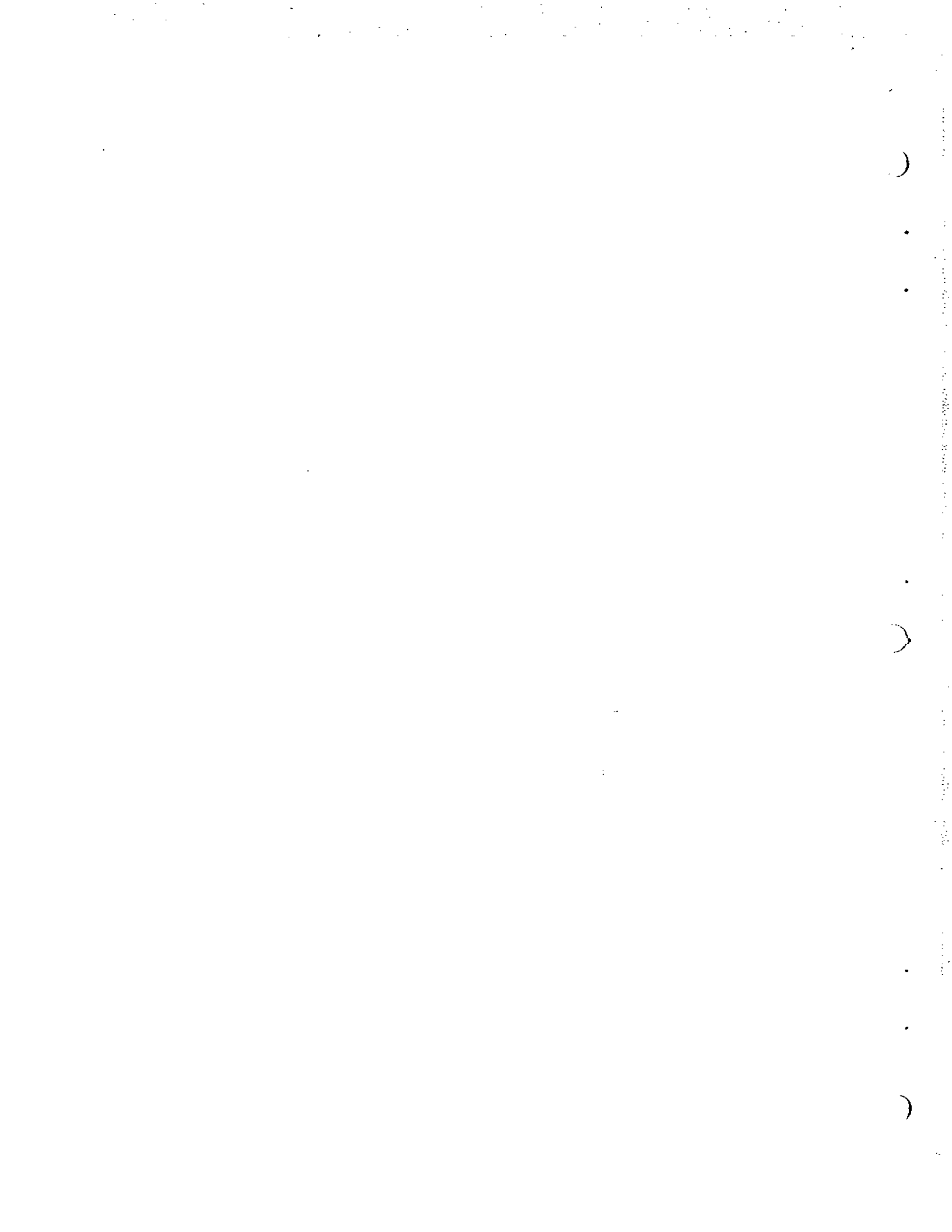


Table 1. Summary of model parameters for triangular current distributions

(2 mm Aluminum)

$T_{BB}$ (keV)	$y_L$	$y_1$	$y_2$	$y_1/y_2$
5	4.7	3.3	8.0	0.41
10	2.3	1.9	4.8	0.40
15	1.6	1.4	3.8	0.37
20	1.2	1.1	3.8	0.29

When the barrier  $\nu_M$  is increased from zero to the peak of the electron distribution ( $0 \leq \nu_M \leq \eta_1$ ), the net current goes from  $J_n/J_o = 1$  down to  $J_n/J_o = 1 - \eta_1/\eta_2$ . Further increases in the barrier height toward the maximum electron energy ( $\eta_1 \leq \nu_M \leq \eta_2$ ) causes the net current to drop to  $J_n/J_o = 0$ .



## V. NUMERICAL RESULTS

The basic formulas, Eq. (10), can now be evaluated using the model distribution given by Eq. (18). Because of the piecewise nature of the triangular distribution, the evaluation divides into three cases.

Case 1:  $\nu_M \leq \eta_1$

$$F_1 = \int_{\nu}^{\nu_M} d\eta \frac{2}{\eta_2} \frac{\eta}{\eta_1} (\eta - \nu)^{1/2} = \frac{4}{\eta_1 \eta_2} F(\nu, \nu_M - \nu) \quad (19a)$$

where

$$F(\nu, x) = x^{3/2} \left( \frac{1}{5} x + \frac{1}{3} \nu \right)$$

$$\begin{aligned} F_2 &= \int_{\nu_M}^{\eta_1} d\eta \frac{2}{\eta_2} \frac{\eta}{\eta_1} [(\eta - \nu)^{1/2} - (\eta - \nu_M)^{1/2}] \\ &\quad + \int_{\eta_1}^{\eta_2} d\eta \frac{2}{\eta_2} \frac{\eta_2 - \eta}{\eta_2 - \eta_1} [(\eta - \nu)^{1/2} - (\eta - \nu_M)^{1/2}] \\ &= \frac{4}{\eta_1 \eta_2} \text{FSC1 } \nu - \frac{4}{\eta_2(\eta_2 - \eta_1)} \text{FSC2 } \nu \end{aligned}$$

where

$$\begin{aligned} \text{FSC1 } \nu &= F(\nu, \eta_1 - \nu) - F(\nu_M, \eta_1 - \nu_M) - F(\nu, \nu_M - \nu) \\ \text{FSC2 } \nu &= F(\nu - \eta_2, \eta_2 - \nu) - F(\nu_M - \eta_2, \eta_2 - \nu_M) \\ &\quad - F(\nu - \eta_2, \eta_1 - \nu) + F(\nu_M - \eta_2, \eta_1 - \nu_M) \end{aligned} \quad (19b)$$

Case 2:  $\nu \leq \eta_1$  and  $\nu_M \geq \eta_1$

$$F_1 = \frac{4}{\eta_1 \eta_2} F(\nu, \eta_1 - \nu) - \frac{4}{\eta_2(\eta_2 - \eta_1)} [F(\nu - \eta_2, \nu_M - \nu) - F(\nu - \eta_2, \eta_1 - \nu)]$$

$$F_2 = - \frac{4}{\eta_2(\eta_2 - \eta_1)} \text{FSC3 } \nu \quad (19c)$$

where

$$\text{FSC3 } \nu = F(\nu - \eta_2, \eta_2 - \nu) - F(\nu_M - \eta_2, \eta_2 - \nu_M) - F(\nu - \eta_2, \nu_M - \nu) \quad (19d)$$

Case 3:  $\nu \geq \eta_1$  and  $\nu_M \geq \eta_1$

$$F_1 = - \frac{4}{\eta_2(\eta_2 - \eta_1)} F(\nu - \eta_2, \nu_M - \nu) \quad (19e)$$

$$F_2 = - \frac{4}{\eta_2(\eta_2 - \eta_1)} \text{FSC3 } \nu \quad (19f)$$

These relations have been incorporated into the APL/360 program titled BBDIØDE which is listed in Fig. 3. This program is suitable for on-line use via the IBM 2741 teletype terminals.

A typical terminal session is shown in Fig. 4. The user first enters the desired values for blackbody temperature TBB (in keV), triangular model parameters Y1 and Y2, and scaling parameter JØL2 (in amperes) by means of the APL operator ←. Access is then gained to the potential program by typing BBDIØDE. The computer responds by requesting a trial value for the potential barrier height NUEM. After this value (usually between 0.1 and 0.3) is entered, the computer types out a short table of

```

VBDDIODE[ ]▽
▽ BDDIODE
  [1]  SOLVES POISSON'S EQN. FOR A DOUBLE DIODE--GGC 9/20/73.
  [2]  V← 0 1 0.05 0.2
  [3]  PREVIOUS TIME←I21
  [4]  NU1←Y1+BETA+(5.69×JOL2*2+3)+TBB
  [5]  NU2←Y2+BETA
  [6]  'SPECIFY TRIAL VALUE FOR NUEM'
  [7]  NUEM←□
  [8]  V RUNGE XO←X1, X1←NUEM×0.99999
  [9]  D←DELTA2 DATA
  [10] →SKIP×\NUEM≥NU1
  [11] JRATIO←1-(NUEM*2)+NU1×NU2
  [12] →OUT
  [13] SKIP:JRATIO+((1-NUEM+NU2)*2)+((1-NU1+NU2)
  [14] OUT:CPU+ 0 60 60 60 TO[(I21)-PREVIOUS TIME
  [15] ' '
  [16] ' '
  [17] 'LEFT= ' ;ZZ1; ' RIGHT= ' ;ZZ2; ' D= ' ;D
  [18] 'JRIGHT+JLEFT= ' ;KAPPA; ' CPU TIME= ' ;CPU; ' M S SS'
  [19] 'Y1= ' ;Y1; ' Y2= ' ;Y2; ' TBB= ' ;TBB; ' NUEM= ' ;NUEM
  [20] 'JO×L*2= ' ;JOL2; ' JNET+JO= ' ;(1-KAPPA)×JRATIO; ' VMAX= ' ;NUEM×TBB×BETA
  [21] (35×D=1)ρ' *'
  [22] 5 1 ρ' *'
▽

▽DELTA2[ ]▽
  [1] Z←DELTA2 X
  [2] XV1←X[ ;2]
  [3] XV2←X[ ;3]
  [4] ZZ1←X[(INDEX XV1);1]
  [5] ZZ2←X[(INDEX XV2);1]
  Z←ZZ1+ZZ2
▽

```

Fig. 3. Listing of APL Programs (For description of use, type BDDIODEHOW.)

```

VFSC[[]]▽
Z+Y FSC X
→5×1X=0
→(0>X)/0
[1] Z+(X+1.5)×((0.2×X)+Y+3)
[2] →0
[3] Z+0
[4]
[5]
▽

VFSC1[[]]▽
Z+VFSC1 X
[1] Z+(X FSC NU1-X)-(NUEM FSC NU1-NUEM)+(X FSC NUEM-X)
▽

VFSC2[[]]▽
Z+VFSC2 X
[1] Z+((X-NU2) FSC NU2-X)-((NUEM-NU2) FSC NU2-NUEM)+((X-NU2) FSC NU1-X)-((
NUEM-NU2) FSC NU1-NUEM)
▽

VFSC3[[]]▽
Z+VFSC3 X
[1] Z+((X-NU2) FSC NU2-X)-((NUEM-NU2) FSC NU2-NUEM)+((X-NU2) FSC NUEM-X)
▽

```

Fig. 3. Listing of APL Programs (For description of use, type BBIDODEHØW.) (Continued)

```

VF1[ ]V
V Z+F1 X
+STEP*10>X
+STEP*1*NUEM>NU1
Z+(4+NU1*NU2)*X FSC NUEM-X
+0
STEP: +STEPD*1X>NU1
Z+(4+NU2)*((+NU1)*X FSC NU1-X)-((+NU2-NU1)*((X-NU2) FSC NUEM-X)-(X-NU2)
FSC NU1-X))
+0
STEPD: Z+-(4+NU2*NU2-NU1)*(X-NU2) FSC NUEM-X
+0
STEP: Z+0
[10] STEP: Z+0
V

```

```

VF2[ ]V
V Z+F2 X
+STEP*10>X
+STEP*1*NUEM>NU1
Z+(4+NU2)*((+NU1)*FSC1 X)-((+NU2-NU1)*FSC2 X)
+0
STEP: Z+-(4+NU2*NU2-NU1)*FSC3 X
+0
STEP: Z+0
V

```

```

VINDEX[ ]V
V Z+INDEX X
Z+(|X)|L/|X
V

```

Fig. 3. Listing of APL Programs (For description of use, type BBDIOEHØW.) (Continued)

```

VSET[ ]V
Z+T SET X
[1] Z1+--((16+9)*((2*F1 X[1])+(1+KAPPA)*F2 X[1]))*0.5
[2] Z2+--((16+9)*((2*KAPPA*F1 X[2])+(1+KAPPA)*F2 X[2]))*
0.5
[3] Z+Z1,Z2
V
VMOSELFIT[ ]V
MODELFIT;A
[1] *FITS BLACKBODY CURRENT DISTR. TO A TRIANGULAR MODEL.
[2] *SPECIFY MASS OF EMITTER IN G/CM*2.*
[3] MASS+[ ]
[4] MUVAL+MU13
[5] EVAL+EE13
[6] EKK+EEK13
[7] YL+(+TBB)*ZERO FCN IN 10 30
[8] Y+0.1*|PLOTARM*YL
[9] CURRENT
[10] YLL+(Y>Y1+Y[RESULT,MAX+[/RESULT])/Y
[11] RL+RESULT[Y,YLL]
[12] CL+RL CLSQ YLL
[13] RL+CL[1]+YLL*CL[2]
[14] Y2+-CL[1]+CL[2]
[15] *IS A PLOT REQUIRED(YES OR NO)?*
[16] +OUT*( 'N'=1+A+[ ]
[17] RPLOT+((Y<Y1)/Y)*RL[1]+Y1),RL
[18] PLOT RESULT AND RPLOT VS Y
[19] OUT: ' '
[20] ' '
[21] *TBB= ;TBB; ' Y1= ;Y1; ' Y2= ;Y2; ' YL= ;YL; '
2)= ;MASS
[22] *PLOT SCALE= ;PLOTARM
V
MASS(G/CM*

```

Fig. 3. Listing of APL Programs (For description of use, type BBDDIODEHØW.) (Continued)



```

VFCN[ ]V
Z+FCN X
Z+1-MASS*MULOOOP X
[1] V

VMULOOOP[ ]V
Z+MULOOOP X;INDEX;EPRIME;MUPRIME
INTERPOLATES LOG MU PIECEWISE BETWEEN ABS. EDGES.
X+.X
INDEX+EKK,1/(X[1]>EKK)/EKK
EPRIME+((EKK[INDEX]<SEVAL)^(EKK[INDEX+1]>EVAL))/EVAL
MUPRIME+MUVAL[EVAL,EPRIME]
Z+1,I+0
LOOP:+0*1((PX)<I+I+1)
Z+Z,*(X[I]) ITP(OMUPRIME) OF(EPRIME)
+LOOP
V

VCURRENT[ ]V
CURRENT
RESULT+1,I+0
STEP1:I+I+1
+0*1,I>0Y
RESULT+RESULT,JINT Y[I]
+STEP1
V

VJINT[ ]V
Z+JINT Y
Z+Y*INTEGRATE JF OVER 1.(20+
[1]

```

Fig. 3. Listing of APL Programs (For description of use, type BBODIODEHØW.) (Continued)

```

VJINT[[]]V
V Z+JINT Y
[1] Z+Y*INTEGRATE JF OVER 1,(20+Y)
V

VJF[[]]V
V Z+JF X
[1] Z+(*-(YL+X*Y)*3)+X*(X*Y)-1
V

VCLSQ[[]]V
V Z+Y CLSQ X,YO;YS;XO;XS
[1] ACONSTRAINED LINEAR LEAST-SQUARES FIT.
[2] Z+(+/(YS+1+Y)-(YO+1+Y)*XS+XO))*+/(1-(XS+XO))*+/(XO+1+X))*
[3] Z+Z.(YO-Z)+XO
V

```

Fig. 3. Listing of APL Programs (For description of use, type BBIODEHØW.) (Concluded)

JOL2+400  
BBDIODE  
SPECIFY TRIAL VALUE FOR NUEM

□:  
.20  
0.2 0.18897 0.18897  
0.4 0.14546 0.14546  
0.6 0.023333 0.023333  
0.8 -0.00084657 -0.00084657  
1 -0.00084657 -0.00084657

LEFT= 0.65 RIGHT= 0.65 D= 1,3  
JRIGHT+JLEFT= 1 CPU TIME= 0 0 15 47 M S SS  
Y1= 1.1 Y2= 3.8 TBB= 20 NUEM= 0.2  
JO×L\*2= 400 JNET+JO= 0 VMAX= 61.78

BBDIODE  
SPECIFY TRIAL VALUE FOR NUEM  
□:

.16  
0.2 0.13233 0.13233  
0.4 0.011408 0.011408  
0.6 -0.012917 -0.012917  
0.8 -0.012917 -0.012917  
1 -0.012917 -0.012917

LEFT= 0.4 RIGHT= 0.4 D= 0.8  
JRIGHT+JLEFT= 1 CPU TIME= 0 0 11 14 M S SS  
Y1= 1.1 Y2= 3.8 TBB= 20 NUEM= 0.16  
JO×L\*2= 400 JNET+JO= 0 VMAX= 49.424

BBDIODE  
SPECIFY TRIAL VALUE FOR NUEM  
□:

.18  
0.2 0.16126 0.16126  
0.4 0.082581 0.082581  
0.6 -0.019402 -0.019402  
0.8 -0.019402 -0.019402  
1 -0.019402 -0.019402

LEFT= 0.5 RIGHT= 0.5 D= 1  
JRIGHT+JLEFT= 1 CPU TIME= 0 0 12 23 M S SS  
Y1= 1.1 Y2= 3.8 TBB= 20 NUEM= 0.18  
JO×L\*2= 400 JNET+JO= 0 VMAX= 55.602

\*\*\*\*\*

Fig. 4. Printout of Typical Terminal Session

values for the distance parameter  $\xi$  (column 1) versus the potential  $v$  on the left and the right of the potential peak (columns 2 and 3 respectively). The last four lines of output provide a summary of data and solutions. The first line gives the location of the left and right grounded plates with respect to the potential peak and the total plate separation  $D$  for the present iteration. The second line gives the ratio of emission currents and the execution time for the computation in minutes, seconds, and sixtieths of a second. The third and fourth lines summarize the input data and give the net current ratio and the maximum potential (in kV). More detailed information on the potential profiles can be obtained by typing DATA. In general, the plate spacing does not turn out to be unity on the first try, so the user must iterate again by typing BBIDODE and repeating the whole process described above. A successful solution for which  $D = 1$  is indicated by a row of asterisks following the last line of output.

The IBM 370/155 execution (CPU) time for each iteration is about 15 sec, which at \$4 per CPU minute amounts to about \$1 per run. Assuming 2 to 4 iterations per case, the costs are about \$2 to \$4 per case. This figure is quite comparable to previous work (Ref. 5), and there is the additional advantage that the user is in the computation loop and can decide how much and what type of information he desires for each case.

A typical family of potential curves for the case of a symmetric diode is shown in Fig. 5. This potential is always centered between the plates and increases with increasing values of the parameter  $J_o l^2$ . Note that for values of  $J_o l^2$  greater than 20 A, the peak potential can exceed 10 kV above ground. For the case of unequal emission, the potential peak moves toward the stronger emitter as shown in Fig. 6, and, for one-sided ( $\kappa = 0$ ) emission and large  $J_o l^2$ , the skewing is quite pronounced.

Numerous runs for  $T_{BB} = 5, 10, \text{ and } 20$  keV and either one-sided or symmetric emission have been summarized in Tables 2 and 3. First, let us examine the dependence of net current  $J_n/J_o$  on  $J_o l^2$  and  $T_{BB}$ . For  $J_o l^2$

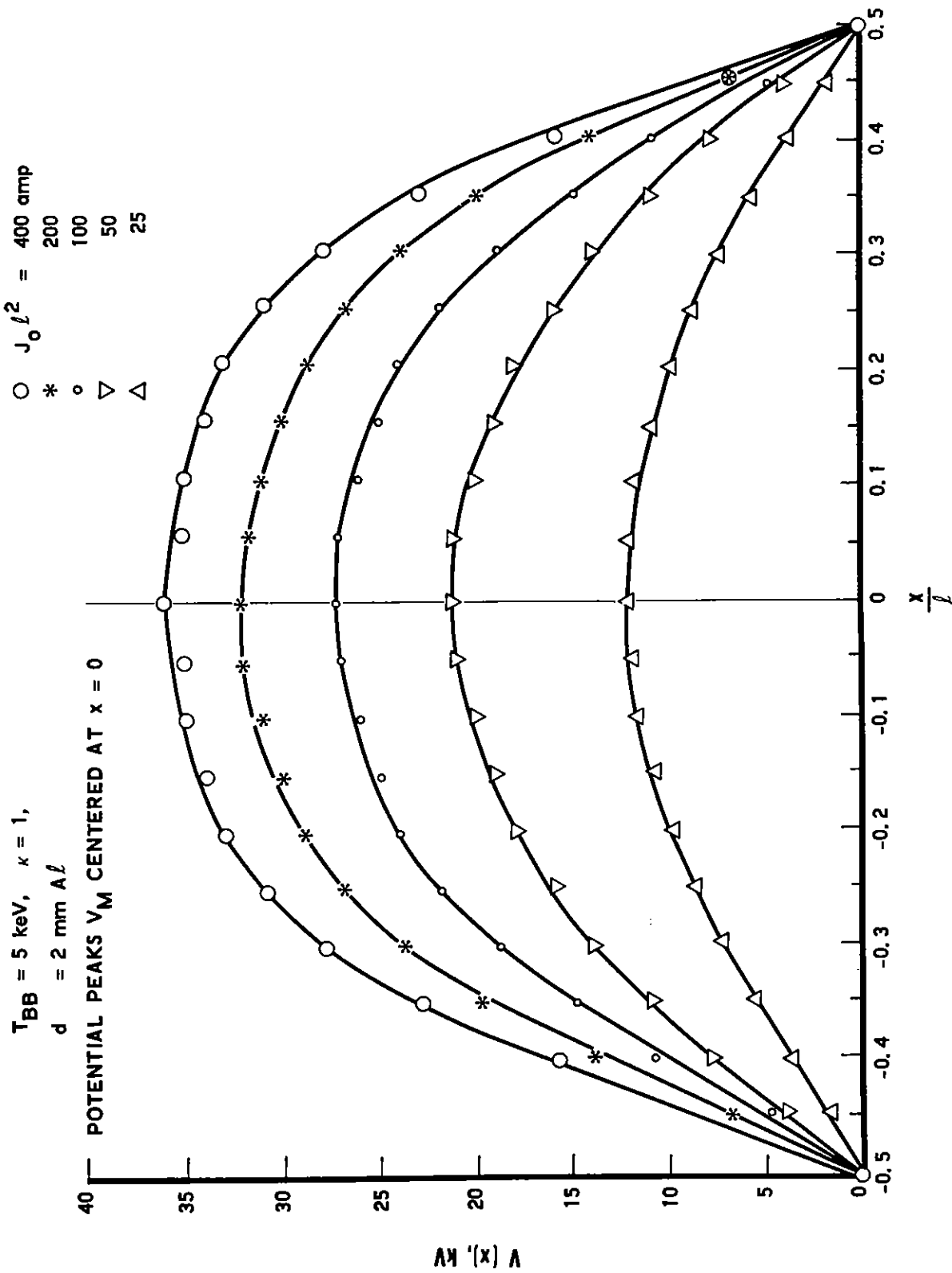


Fig. 5. Potential Curves for Symmetric Diode with  $J_0 l^2$  as a Parameter

$T_{BB} = 5, J_0 l^2 = 100, d = 2 \text{ mm } Al$

POTENTIAL PEAKS  $V_M$  CENTERED AT  $x = 0$

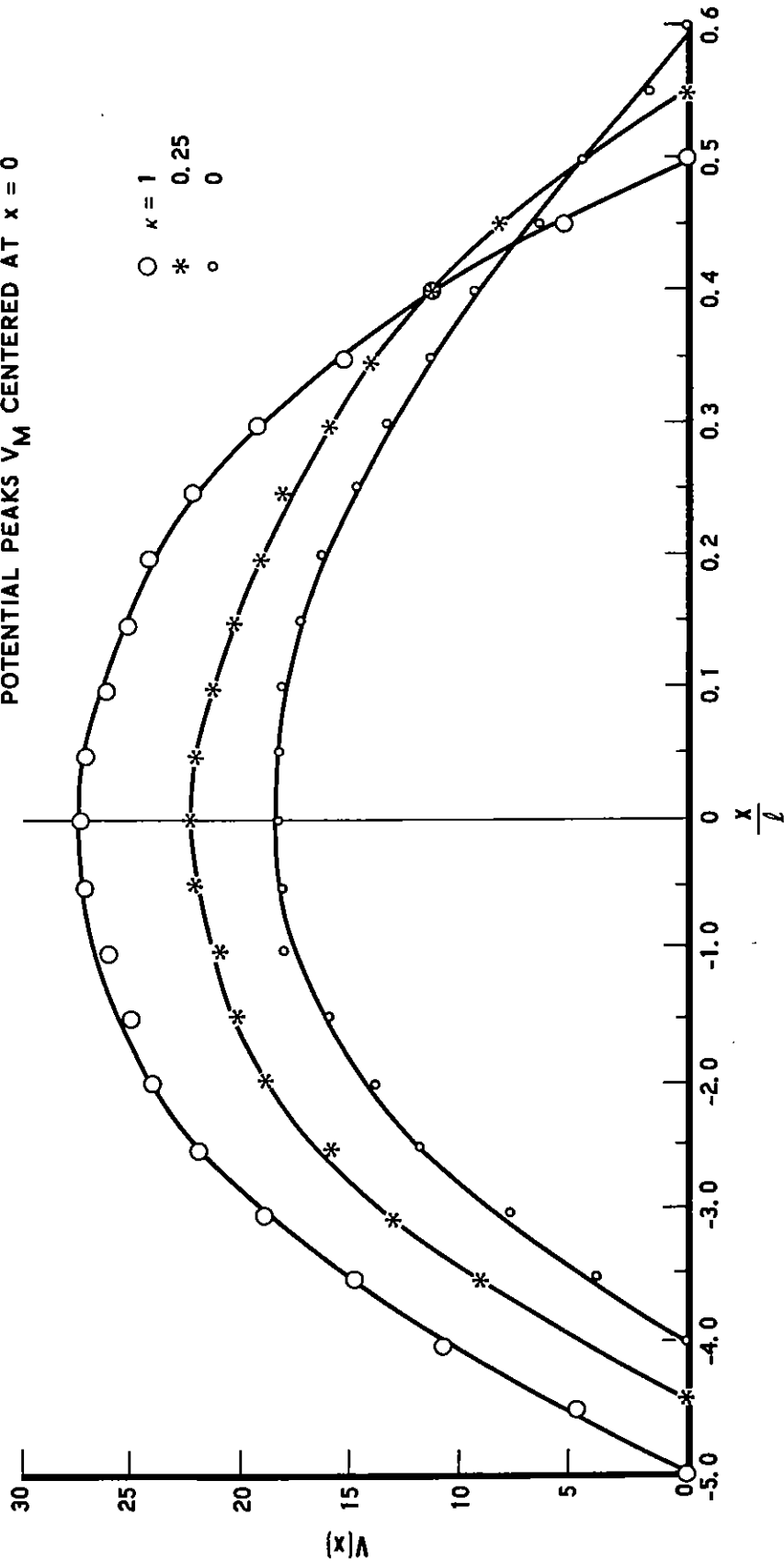


Fig. 6. Potential Curves with  $\kappa$  as a Parameter  
 ( $\kappa$  = ratio of backward to forward emission,  
 e.g.,  $\kappa = 1$  denotes symmetric emission.)

Table 2. Peak potentials and net currents for a single diode  
(MASS = 2 mm Al,  $\kappa = 0$ )

$T_{BB}$ (keV)	$J_o l^2$ (A)	$v_M$	$J_n/J_o$	$V_M$ (kV)
5	25	0.10	0.97	4.9
	50	0.14	0.87	10.8
	100	0.16	0.60	19.6
	200	0.135	0.34	26.3
	400	0.105	0.17	32.4
10	25	0.11	0.96	5.4
	50	0.15	0.80	11.6
	100	0.15	0.50	18.4
	200	0.125	0.26	24.3
	400	0.093	0.14	28.7
20	25	0.085	0.99	4.1
	50	0.11	0.96	8.5
	100	0.14	0.82	17.2
	200	0.15	0.53	29.2
	400	0.125	0.34	38.6

Table 3. Peak potentials from a symmetric double diode  
(MASS = 2 mm Al,  $\kappa = 1$ ,  $J_n/J_o = 0$ )

$T_{BB}$ (keV)	$J_o l^2$ (A)	$v_M$	$V_M$ (kV)
5	25	0.25	12.2
	50	0.27	20.9
	100	0.22	27.0
	200	0.165	32.1
	400	0.115	35.5
10	25	0.20	9.7
	50	0.26	20.1
	100	0.24	29.4
	200	0.185	36.0
	400	0.132	40.8
20	25	0.16	7.8
	50	0.22	17.0
	100	0.24	29.4
	200	0.22	42.8
	400	0.18	55.6



greater than 50 or 100 A, the net current in an unequal double-diode drops significantly below unity. The dependence on the radiation temperature enters through the ratio  $y_1/y_2$ , which (as seen from Table 1) does not vary greatly as  $T_{BB}$  is quadrupled in value. The most sensitive dependence of  $J_n/J_o$ , as indicated by Eq. (18), is on  $J_o \ell^2$  via the dimensionless barrier height  $\nu_M$ . Note, however, that for each fixed temperature, the  $\nu_M$  values pass through a maximum, so that similar  $J_n/J_o$  values result only if we compare both the upper or lower branches of Eq. (18) in both cases.

As has been previously pointed out, the values of  $\nu_M$  do not change markedly with  $J_o \ell^2$  (e.g., a fourfold increase in  $J_o \ell^2$  from 25 to 100 results in a 60 percent change in  $\nu_M$  for the case  $T_{BB} = 5$  keV). Since  $\nu_M = V_M/V_o$  and  $V_o = 5.69 (J_o \ell^2)^{2/3}$ , it is evident that the peak potential is given by  $V_M = \beta (J_o \ell^2)^{2/3}$  where  $\beta$  is around 0.5 to 1.0 for the range of parameters in Table 2. On the other hand, the classic Child-Langmuir solution for a centered potential is  $V_M = 5.69 (J_o \ell^2/4)^{2/3} = 2.26 (J_o \ell^2)^{2/3}$ . Therefore, the potential solutions for arbitrarily large values of  $J_o \ell^2$  are not correctly given by the usual analytical results. This is because we are dealing with a spread in electron energies rather than a monoenergetic distribution. Nevertheless, neglecting the slow variation of  $\nu_M$  with  $J_o \ell^2$ , the scaling law for  $V_M$  with  $J_o \ell^2$  is approximately that predicted by Child and Langmuir. Only the proportionality constant is different.

For actual IEMP studies, these results can be extrapolated graphically, or additional computer runs can be readily made.

)

.

.

.

)

.

.

)

## REFERENCES

1. H. F. Ivey, in Advances in Electronics and Electron Physics, Ed: L. Marton, Vol. VI, Academic Press, Inc., N.Y., 138-251 (1954).
2. C. K. Birdsall and W. B. Bridges, Electron Dynamics of Diode Regions, Academic Press, Inc., N.Y. (1966).
3. E. P. Denisov, V. N. Schemeleev, A. N. Mezhevich, and M. A. Rumsh, Soviet Physics--Solid State 6, 1047 (1965).
4. W. L. Chadsey and I. Kohlberg, IEEE Trans. Nucl. Sci. NS-18, 150 (1971).
5. A. J. Woods and E. P. Wenaas, Proc. IEMP Symp., DNA-3098P, p. 23-3 (4 June 1973) (Secret-RD).
6. T. A. Dellin and C. J. MacCallum, A Handbook of Photo-Compton Current Data, SLL-RR-720086, Sandia Laboratories, Albuquerque, New Mexico (December 1972).
7. R. D. Evans, The Atomic Nucleus, McGraw-Hill Book Co., N.Y., Ch. 21 and 24 (1955).

